Journal of Applied Mechanics and Technical Physics, Vol. 51, No. 4, pp. 489–496, 2010

MATHEMATICAL MODELING OF VISCOUS GAS FLOW IN A DOUBLY CONNECTED VOLUME WITH PERFORATED WALLS

A. M. Lipanov and A. N. Semakin

UDC 533.6.011.3

A numerical method is proposed for computing viscous gas flow in an initial doubly connected domain which is a volume having perforated walls and enclosing a sphere. The types of subdomains (finite volumes) into which the initial domain can be divided are considered. For each type of finite volume, there is a curvilinear coordinate system. Results of flow computation for Re = 100 *and 500, and* $M = 0.6$ *are given.*

Key words: *doubly connected domain, finite volume, viscous gas, system of equations of hydromechanics, curvilinear coordinate system.*

Introduction. The problem of calculating the fields of hydromechanical parameters for multiconnected domains is encountered in many practical applications such as drying of bulk grain by warm air flow, filtration of viscous fluids through pores in rock, purification of polluted or gaseous media by filtration through a layer of particles occupying some volume, etc. Traditionally, such spatial problems are solved by reducing a multiply connected domain to a simply connected domain, introducing a porosity factor, filtration rate, etc. [1]. In [2], an alternative approach is proposed which allows hydromechanical parameters to be computed directly for multiply connected domains without additional assumptions. In the present work, this approach is applied to doubly connected domains.

1. Formulation of the Problem. Let us consider a perforated volume Q in the shape of a rectangular parallelepiped with one inlet and two outlets. The inlet is in the middle of the front face, and the outlets are on the vertical symmetry axis of the rear face. The inlet and both outlets have a circular shape. In this volume there is a sphere which can touch any of its walls. Figure 1 shows an example of the domain considered in which the sphere is at the center of the volume Q. A viscous gas passes through the inlet hole. It is required to compute the parameters of the gas passing through this volume.

2. Finite Volumes. We use a global Cartesian coordinate system (X, Y, Z) to consider the entire initial domain and divide this domain into N_{fv} subdomains or finite volumes (FVs). The shapes of all FVs can be classified into five standard types: rectangular, spherical, pyramidal, circular, and cylindrical (Fig. 2). The rectangular FV is a rectangular parallelepiped. The spherical FV is used to enclose space in the vicinity of the sphere away from the side walls of the volume Q. One of the six faces of the spherical volume is the surface of the sphere. The pyramidal FV has a wedge shape and encloses space near the point of contact of the sphere with one of the wall sides of the volume Q. One face of the circular FV is part of the cylindrical surface. The cylindrical FV is a cylinder used to describe the inlet and the outlets.

In each of the FVs, we introduce a Cartesian coordinate system (x, y, z) which is defined by the coordinate origin $O(a_0^1, a_0^2, a_0^3)$ and the basis vectors $\boldsymbol{i} = (a_1^1, a_1^2, a_1^3)$, $\boldsymbol{j} = (a_2^1, a_2^2, a_2^3)$, and $\boldsymbol{k} = (a_3^1, a_3^2, a_3^3)$ in the global coordinate system (X, Y, Z). Then, the local (x, y, z) and global (X, Y, Z) coordinates of a point are connected by the following relations [3]:

Institute of Applied Mechanics, Ural Division, Russian Academy of Sciences, Izhevsk 426067; artesemaki@yandex.ru. Translated from Prikladnaya Mekhanika i Tekhnicheskaya Fizika, Vol. 51, No. 4, pp. 48–56, July–August, 2010. Original article submitted February 13, 2008; revision submitted November 18, 2009.

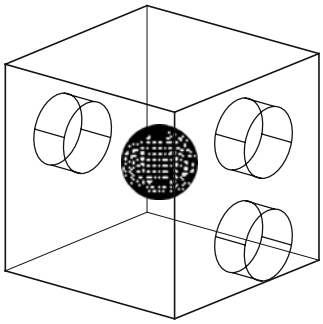

Fig. 1. Example of the computational domain.

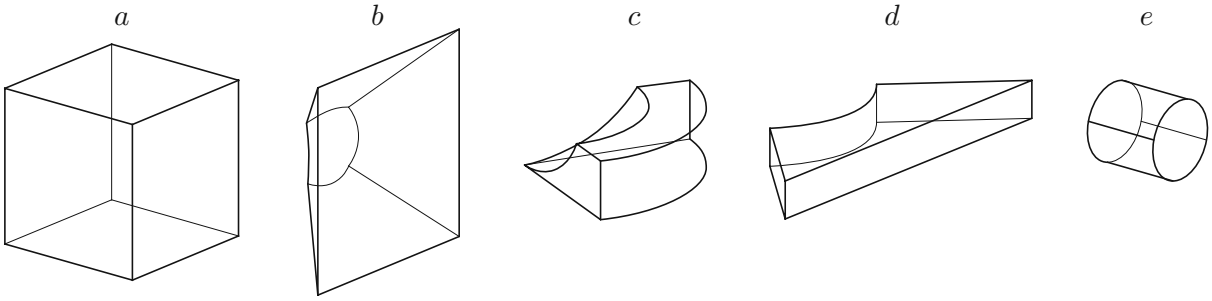

Fig. 2. Types of finite volumes: rectangular (a), spherical (b), pyramidal (c), circular (d), and cylindrical (e).

$$(x,y,z)\to(X,Y,Z): \qquad \boldsymbol{R}=\boldsymbol{a}_0+\boldsymbol{a}_1x+\boldsymbol{a}_2y+\boldsymbol{a}_3z,$$

$$(X,Y,Z)\to(x,y,z): \qquad \boldsymbol{r}=\boldsymbol{a}^1X+\boldsymbol{a}^2Y+\boldsymbol{a}^3Z-\boldsymbol{b}.$$

Here

$$\boldsymbol{R}=(X,Y,Z), \qquad \boldsymbol{r}=(x,y,z), \qquad \boldsymbol{a}_0=(a_0^1,a_0^2,a_0^3),$$

$$\boldsymbol{a}_1=(a_1^1,a_1^2,a_1^3), \qquad \boldsymbol{a}_2=(a_2^1,a_2^2,a_2^3), \qquad \boldsymbol{a}_3=(a_3^1,a_3^2,a_3^3),$$

$$\boldsymbol{a}^1=(a_1^1,a_2^1,a_3^1), \qquad \boldsymbol{a}^2=(a_1^2,a_2^2,a_3^2), \qquad \boldsymbol{a}^3=(a_1^3,a_2^3,a_3^3),$$

$$\boldsymbol{b}=(\boldsymbol{a}_1\cdot\boldsymbol{a}_0,\boldsymbol{a}_2\cdot\boldsymbol{a}_0,\boldsymbol{a}_3\cdot\boldsymbol{a}_0).$$

In all types of FVs, except in the rectangular FV, we should introduce a curvilinear coordinate system (ξ,η,ζ) in which this FV can be represented as a parallelepiped. According to [4–6], let us define the formulas of the transformation to curvilinear coordinates:

— for the spherical FV,

$$\xi=\sqrt{x^2+y^2+z^2}, \qquad \eta=-y/x, \qquad \zeta=-z/x, \tag{1}$$

where $-1\leqslant\eta\leqslant1$ and $-1\leqslant\zeta\leqslant1$;

— for the pyramidal FV,

$$\xi=(x^2+y^2+z^2)/\sqrt{x^2+z^2}, \qquad \eta=2y/(x^2+y^2+z^2), \qquad \zeta=-z/x, \tag{2}$$

where $0\leqslant\eta\leqslant1/r$ and $-1\leqslant\zeta\leqslant1$ (r is the radius of the sphere);

— for the circular FV,

$$\xi=\sqrt{x^2+z^2}, \qquad \eta=y, \qquad \zeta=-z/x, \tag{3}$$

where $-1\leqslant\zeta\leqslant1$;

— for the cylindrical FV,

$$\xi = x, \qquad \eta = \sqrt{y^2 + z^2}, \qquad \zeta = \arctan\,(z/y) + \pi k, \tag{4}$$

where $-\pi \leqslant \zeta \leqslant \pi$.

During the construction, the computational meshes were compressed (refined) toward the surface of the sphere and toward the front and rear faces of the volume Q.

3. System of Equations of Hydromechanics. For each of the FV in its local Cartesian coordinate system, we write the system of equations of hydromechanics in nondimensional form [7, 8]:

$$\frac{\partial \rho}{\partial t} + \frac{1}{2}\Big(u\,\frac{\partial \rho}{\partial x} + v\,\frac{\partial \rho}{\partial y} + w\,\frac{\partial \rho}{\partial z} + \frac{\partial \rho u}{\partial x} + \frac{\partial \rho v}{\partial y} + \frac{\partial \rho w}{\partial z}\Big) + \frac{1}{2}\,\rho\,\mathrm{div}\,(\boldsymbol{V}) = 0,$$

$$\frac{\partial u}{\partial t} + \frac{1}{2}\Big(u\,\frac{\partial u}{\partial x} + v\,\frac{\partial u}{\partial y} + w\,\frac{\partial u}{\partial z} + \frac{\partial u^2}{\partial x} + \frac{\partial uv}{\partial y} + \frac{\partial uw}{\partial z}\Big) - \frac{1}{\rho\,\mathrm{Re}}\Big(\frac{\partial^2 u}{\partial x^2} + \frac{\partial^2 u}{\partial y^2} + \frac{\partial^2 u}{\partial z^2}\Big)$$

$$= -\frac{1}{\rho k \mathrm{M}^2}\,\frac{\partial p}{\partial x} + \frac{1}{2}\,u\,\mathrm{div}\,(\boldsymbol{V}) + \frac{1}{3\rho\,\mathrm{Re}}\,\frac{\partial}{\partial x}\,\mathrm{div}\,(\boldsymbol{V}),$$

$$\frac{\partial v}{\partial t} + \frac{1}{2}\Big(u\,\frac{\partial v}{\partial x} + v\,\frac{\partial v}{\partial y} + w\,\frac{\partial v}{\partial z} + \frac{\partial uv}{\partial x} + \frac{\partial v^2}{\partial y} + \frac{\partial vw}{\partial z}\Big) - \frac{1}{\rho\,\mathrm{Re}}\Big(\frac{\partial^2 v}{\partial x^2} + \frac{\partial^2 v}{\partial y^2} + \frac{\partial^2 v}{\partial z^2}\Big)$$

$$= -\frac{1}{\rho k \mathrm{M}^2}\,\frac{\partial p}{\partial y} + \frac{1}{2}\,v\,\mathrm{div}\,(\boldsymbol{V}) + \frac{1}{3\rho\,\mathrm{Re}}\,\frac{\partial}{\partial y}\,\mathrm{div}\,(\boldsymbol{V}), \tag{5}$$

$$\frac{\partial w}{\partial t} + \frac{1}{2}\Big(u\,\frac{\partial w}{\partial x} + v\,\frac{\partial w}{\partial y} + w\,\frac{\partial w}{\partial z} + \frac{\partial uw}{\partial x} + \frac{\partial vw}{\partial y} + \frac{\partial w^2}{\partial z}\Big) - \frac{1}{\rho\,\mathrm{Re}}\Big(\frac{\partial^2 w}{\partial x^2} + \frac{\partial^2 w}{\partial y^2} + \frac{\partial^2 w}{\partial z^2}\Big)$$

$$= -\frac{1}{\rho k \mathrm{M}^2}\,\frac{\partial p}{\partial z} + \frac{1}{2}\,w\,\mathrm{div}\,(\boldsymbol{V}) + \frac{1}{3\rho\,\mathrm{Re}}\,\frac{\partial}{\partial z}\,\mathrm{div}\,(\boldsymbol{V}),$$

$$\frac{\partial T}{\partial t} + \frac{1}{2}\Big(u\,\frac{\partial T}{\partial x} + v\,\frac{\partial T}{\partial y} + w\,\frac{\partial T}{\partial z} + \frac{\partial uT}{\partial x} + \frac{\partial vT}{\partial y} + \frac{\partial wT}{\partial z}\Big) - \frac{k}{\rho\,\mathrm{Re}\,\mathrm{Pr}}\Big(\frac{\partial^2 T}{\partial x^2} + \frac{\partial^2 T}{\partial y^2} + \frac{\partial^2 T}{\partial z^2}\Big)$$

$$= -\frac{k-1}{\rho}\,p\,\mathrm{div}\,(\boldsymbol{V}) + \frac{1}{2}\,T\,\mathrm{div}\,(\boldsymbol{V}) + \frac{k(k-1)\mathrm{M}^2}{\rho\,\mathrm{Re}}\Big[2\Big(\frac{\partial u}{\partial x}\Big)^2 + 2\Big(\frac{\partial v}{\partial y}\Big)^2 + 2\Big(\frac{\partial w}{\partial z}\Big)^2$$

$$+ \Big(\frac{\partial u}{\partial y} + \frac{\partial v}{\partial x}\Big)^2 + \Big(\frac{\partial u}{\partial z} + \frac{\partial w}{\partial x}\Big)^2 + \Big(\frac{\partial v}{\partial z} + \frac{\partial w}{\partial y}\Big)^2 - \frac{2}{3}\,(\mathrm{div}\,(\boldsymbol{V}))^2\Big].$$

Here $\boldsymbol{V} = (u, v, w)$ is the velocity vector, p, ρ, and T are the pressure, density, and temperature, Re is the Reynolds number, $\mathrm{Pr} = 1$ is the Prandtl number, M is the Mach number, $k = 1.4$ is the ratio of the isobar heat capacity C_p and the isochoric heat capacity C_v, and $\mathrm{div}\,(\boldsymbol{V}) = \partial u/\partial x + \partial v/\partial y + \partial w/\partial z$ is the velocity divergence.

System (5) is closed by the nondimensional equation of state

$$p = \rho T. \tag{6}$$

The method of nondimensionalizing of Eqs. (5) and (6) is given in [9].

For transformation to curvilinear coordinates in the initial equations, it is necessary to make a change of variables. For instance, the first derivative with respect to x is replaced by the expression

$$\frac{\partial W}{\partial x} = \frac{\partial W}{\partial \xi}\,\xi_x + \frac{\partial W}{\partial \eta}\,\eta_x + \frac{\partial W}{\partial \zeta}\,\zeta_x.$$

Similar expressions can be written for the derivatives with respect to y and z. The sum of the second derivatives is changed as follows:

$$\frac{\partial^2 W}{\partial x^2}+\frac{\partial^2 W}{\partial y^2}+\frac{\partial^2 W}{\partial z^2}=\frac{\partial^2 W}{\partial \xi^2}\,\nabla\xi\nabla\xi+\frac{\partial^2 W}{\partial \eta^2}\,\nabla\eta\nabla\eta+\frac{\partial^2 W}{\partial \zeta^2}\,\nabla\zeta\nabla\zeta$$

$$+2\,\frac{\partial^2 W}{\partial \xi\,\partial \eta}\,\nabla\xi\nabla\eta+2\,\frac{\partial^2 W}{\partial \xi\,\partial \zeta}\,\nabla\xi\nabla\zeta+2\,\frac{\partial^2 W}{\partial \eta\,\partial \zeta}\,\nabla\eta\nabla\zeta$$

$$+\frac{\partial W}{\partial \xi}\,(\xi_{xx}+\xi_{yy}+\xi_{zz})+\frac{\partial W}{\partial \eta}\,(\eta_{xx}+\eta_{yy}+\eta_{zz})+\frac{\partial W}{\partial \zeta}\,(\zeta_{xx}+\zeta_{yy}+\zeta_{zz}). \tag{7}$$

Here $\nabla\xi=(\xi_x,\xi_y,\xi_z)$, $\nabla\eta=(\eta_x,\eta_y,\eta_z)$, $\nabla\zeta=(\zeta_x,\zeta_y,\zeta_z)$, $\nabla\xi\nabla\eta$, $\nabla\xi\nabla\zeta$, and $\nabla\eta\nabla\zeta$ are the scalar products of the vectors.

Substituting expressions (7) into the initial equations, we have the system of equations of hydromechanics in curvilinear coordinates. The values of the derivatives ξ_x, η_x, ζ_x, etc. are computed analytically by transforming the coordinates (1)–(4) for various types of FVs.

4. Initial and Boundary Conditions. To solve the equations of hydromechanics, it is necessary to specify the initial and boundary conditions. As the initial conditions, we use the following values: $u=v=w=0$ and $p=\rho=T=1$. The boundary conditions of the multiply connected domain are specified according to [2, 10]. If any of the faces of the FV reach the boundary of the multiply connected domain, on these faces we specify one of the boundary condition given in [2, 10].

The partial derivatives with respect to spatial directions at the nodes of the computational mesh are calculated using the method of undetermined coefficients, which allows these derivatives to be calculated with any order of accuracy. To determine the derivative at a specified point using this method, it is necessary to know the values of the required function at several neighboring nodes. Therefore, in the calculation of the derivatives at the points near the boundary of the FV, it is necessary to enter neighboring FVs. As a rule, the computational meshes in two adjacent FVs are not consistent, i.e., when we enter the neighboring FV, the considered points may not coincide with the calculation points of the computational mesh of this FV. Therefore, to determine the values at the required points, it is necessary to perform an interpolation by the known values of these quantities at the calculation points of the neighboring FV.

5. Interpolation. The unknown value of the quantity f at the point $\boldsymbol{x}^0=(x^0,y^0,z^0)$ is determined through the known values of this quantity at the points $\boldsymbol{x}^k=(x^k,y^k,z^k)$ $(k=1,N)$ with the use of a truncated Fourier series constructed using a system of orthogonal polynomials [11]:

$$f(\boldsymbol{x}^0)=\sum_{i+j+k=0}^{n} c_{ijk}\psi_{ijk}(\boldsymbol{x}^0),\qquad c_{ijk}=(\psi_{ijk}(\boldsymbol{x}),f(\boldsymbol{x})).$$

The system of orthogonal polynomial $\psi_{ijk}(\boldsymbol{x})$ can be obtained sequentially from the formulas

$$\psi_{ijk}(\boldsymbol{x})=\varphi_{ijk}(\boldsymbol{x})/\|\varphi_{ijk}(\boldsymbol{x})\|,$$

$$\varphi_{000}=1,\qquad \varphi_{ijk}(\boldsymbol{x})=x\psi_{i-1jk}(\boldsymbol{x})+y\psi_{ij-1k}(\boldsymbol{x})+z\psi_{ijk-1}(\boldsymbol{x})+\sum_{M}\alpha_{mnl}\psi_{mnl}(\boldsymbol{x}),$$

$$\alpha_{mnl}=-(x\psi_{i-1jk}(\boldsymbol{x})+y\psi_{ij-1k}(\boldsymbol{x})+z\psi_{ijk-1}(\boldsymbol{x}),\psi_{mnl}(\boldsymbol{x})),$$

where M is the set of the constructed polynomials.

The scalar product and the norm in the polynomial space are determined as follows:

$$(f(\boldsymbol{x}),g(\boldsymbol{x}))=\sum_{k=1}^{N} f(\boldsymbol{x}^k)g(\boldsymbol{x}^k),\qquad \|f(\boldsymbol{x})\|=\sqrt{(f(\boldsymbol{x}),f(\boldsymbol{x}))}.$$

In the computations, we set $n=2$ and $N=10$, which is equivalent to the interpolation by a second-order polynomial. The points $\boldsymbol{x}^k$ were chosen so as to satisfy the condition $\|\varphi_{ijk}(\boldsymbol{x})\|\geqslant 10^{-4}$ for all $\varphi_{ijk}(\boldsymbol{x})$.

6. Computational Method for Solving the Equations of Hydromechanics. The equations of hydromechanics were integrated using the Runge–Kutta method of the second order of accuracy [11], and the partial derivatives with respect to spatial variables were calculated using a central difference mesh of an arbitrary order of accuracy [9]. To eliminate nonphysical oscillations, we added an artificial dissipation to the computational mesh [12].

TABLE 1

Sphere Resistance Coefficient versus the Number of Calculation Nodes and the Order of Accuracy of the Difference Mesh for $\mathrm{Re} = 100$

N_p	C_x		
	$N_c = 2$	$N_c = 4$	$N_c = 6$
$6 \times 30 \times 13 \times 13$	1.502	1.130	1.099
$6 \times 40 \times 17 \times 17$	1.320	1.114	1.098
$6 \times 50 \times 23 \times 23$	1.246	1.096	1.092

TABLE 2

Sphere Resistance Coefficient versus Reynolds Number for $N_p = 6 \times 30 \times 13 \times 13$ and the Sixth Order of Accuracy

Re	C_x	C_x^t
50	1.582	1.609
100	1.099	1.121
250	0.723	0.756
500	0.601	0.597
1000	0.536	0.495

After a next time step is performed, it is necessary to transfer the values of the hydromechanical parameters (ratio, density, and temperature) from one FV to another. Since density and temperature are scalar quantities, their values do not depend on the orientation of the local coordinate systems of various FVs. However, during transition from one coordinate system to another, the components of the velocity vector change; therefore, when the velocity vector components are transferred from one FV to another, they are first transformed to the global coordinate system according to the formulas [3]

$$U = a_1^1 u + a_2^1 v + a_3^1 w, \qquad V = a_1^2 u + a_2^2 v + a_3^2 w, \qquad W = a_1^3 u + a_2^3 v + a_3^3 w,$$

and then they are transferred from the global coordinate system to a local system of the other FV:

$$u = a_1^1 U + a_1^2 V + a_1^3 W, \qquad v = a_2^1 U + a_2^2 V + a_2^3 W, \qquad w = a_3^1 U + a_3^2 V + a_3^3 W.$$

The transition coefficients a_i^j are specified above.

7. Computation Results. As a test problem we considered the problem of flow over a sphere. The computation domain is a sphere of radius 7.8 which encloses a sphere of radius 0.5. This computation domain is divided into six spherical FVs. The sphere resistance coefficient C_x was employed as the criterion of calculation accuracy. For the chosen Mach number of the incident flow $\mathrm{M} = 0.1$, the computation results should be close to the data for an incompressible fluid [13]. Consequently, the values of C_x obtained by calculations can be compared with the standard dependence of the resistance coefficient of the incompressible-fluid sphere on the Reynolds number approximated by the formula [14]

$$C_x = 24(1 + 0.25\sqrt{\mathrm{Re}} + 0.0117\,\mathrm{Re})/\,\mathrm{Re}, \qquad 1 \leqslant \mathrm{Re} \leqslant 1000. \tag{8}$$

Table 1 shows the dependence of the sphere resistance coefficient on the number of calculation nodes N_p and the order of accuracy of the difference scheme in the spatial variables N_c for $\mathrm{Re} = 100$. From Table 1, it follows that in the calculations using the difference scheme of the sixth order of accuracy, the value of C_x obtained on the most coarse mesh almost does not change with a further increase in the number of nodes (the changes in the third decimal digit are likely due to errors in the calculation of the resistance coefficient), i.e., to determine the sphere resistance coefficient in the calculations by the sixth-order scheme, it is sufficient to use the most coarse difference mesh. Table 2 shows calculation results of the resistance coefficient for various values of the Reynolds number on a $6 \times 30 \times 13 \times 13$ mesh using the scheme of the sixth order of accuracy. It is evident that values of the resistance coefficient C_x obtained in the calculations are in good agreement with the values of the resistance coefficient C_x^t obtained using the approximate dependence (8).

For $\mathrm{Re} = 50$, 100, and 250, we measured the length of the separation zone behind the sphere (0.4, 0.8, and 1.1, respectively) and the flow separation angle (41°, 52°, and 65°, respectively). The results agree with the data of [14].

Next, the sphere was placed in a volume with one inlet and two outlets (the length, height, and width of the volume are 3, and the inlet and outlet radii, the inlet length, and the sphere radius are 0.5). In the calculations, we considered three variants of sphere position: 1) the sphere is at the center of the channel; 2) the sphere is below the center of the channel at a distance of one radius; 3) the sphere touches the lower plane of the channel.

In variant No. 1, the length of the outlets was set equal to 0.5, and in the remaining variants it was set equal to 0.2. The calculations were performed for $\mathrm{Re} = 100$ and 500 and $\mathrm{M} = 0.6$. For $\mathrm{Re} = 100$, the solution convergence was investigated as a function of the number of calculation nodes of the difference mesh in variant No. 1.

TABLE 3

Some Flow Characteristics for Variant No. 1 at $\mathrm{Re} = 100$

N_p	C_x	$\omega_{\max}$	α_u, deg	α_p, deg	m_1	m_2
49,338	1.165	14.588	65.74	113.20	1.132	1.177
378,918	1.170	14.670	66.14	113.63	1.118	1.099

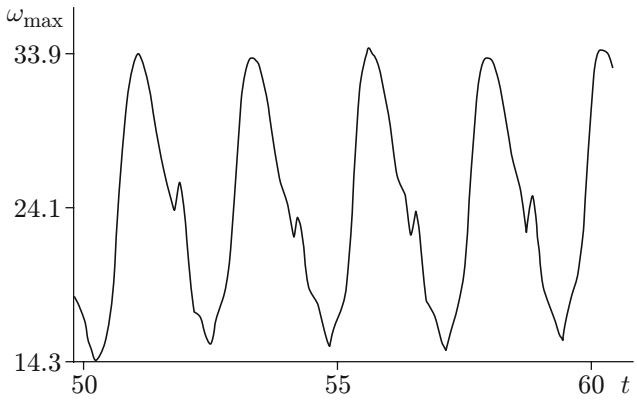

Fig. 3

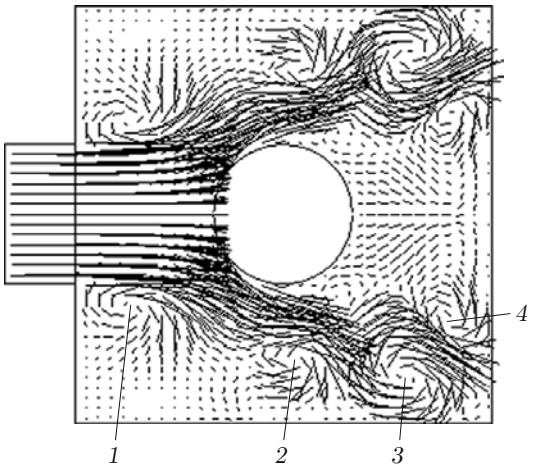

Fig. 4

Fig. 3. Time dependence of the maximum of the vorticity modulus for $\mathrm{Re} = 500$ for variant No. 1.

Fig. 4. Velocity field in the section XZ at $Y = 1.5$ for variant No. 1: forming vortex (1), vortex moving along the gas jet (2), stationary vortex (3), and small periodically appearing vortices (4).

Schemes of the second, the fourth and the sixth orders of accuracy were considered on meshes with $N_p = 49{,}338$ and $N_p = 378{,}918$ nodes. The calculations showed that, to obtain a convergent solution, it is sufficient to use a difference scheme of the fourth order of accuracy on the most coarse mesh. Figure 3 shows values of some flow parameters computed by the scheme of the fourth order of accuracy ($\omega_{\max}$ is the maximum of the vorticity modulus, α_u and α_p are the angle of flow separation from the sphere and the angle corresponding to the minimum pressure on the sphere reckoned from the rear critical point of the sphere, and m_1 and m_2 are the mass flows at the inlet and outlet). According to Table 3, $\alpha_p > \alpha_u$, which corresponds to boundary-layer theory [7]. On the coarse mesh, the difference of the values of m_1 and m_2 is 4%, and on the fine mesh, it is 1.7% with respect to the smallest of the quantities m_1 and m_2.

According to the mass conservation law, stationary flow without sources and sinks should satisfy the condition $m_1 = m_2$. In this case, the error of the satisfaction of the mass conservation law is due to the error of the numerical integration in the calculations of mass flow rate, the error of the interpolation (the values of hydromechanical variables are transferred from one finite volume to another by polynomial interpolation which was performed without taking the conservation laws into account), and the error of the difference scheme (the difference scheme is based on the equations of hydromechanics in symmetric form, and, hence, is not conservative, i.e., it implements the integral conservation laws with a certain error).

The aforesaid leads to the conclusion that the proposed calculation method provides results that are in good agreement with both the theory and experiment.

For $\mathrm{Re} = 100$, a stationary solution is obtained in all cases. The gas flows into the volume as a clearly defined jet which keeps its shape until collision with the sphere. In variant Nos. 1 and 2, flowing over the sphere, this jet transforms takes the shape of a dome whose edges are directed toward the outlets. In variant No. 3, the jet only touches the sphere and continues to move toward the outlets without significant changes, only slightly moving to the upper wall. Large vortices are formed on the left and on the right of the gas jet flow into the volume and behind the sphere.

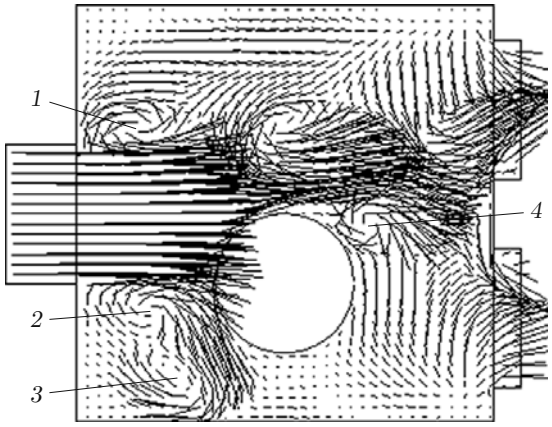

Fig. 5

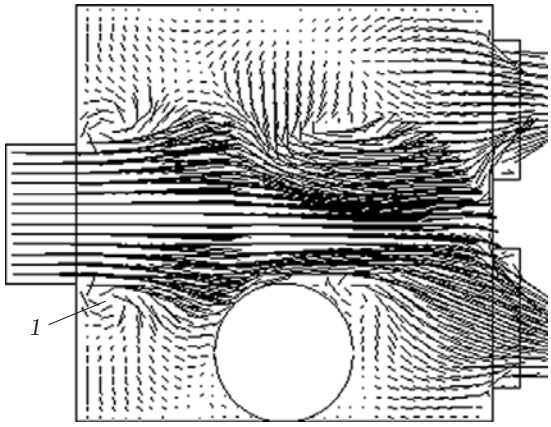

Fig. 6

Fig. 5. Velocity field in the section XY at $Z = 1.5$ for variant No. 2: periodically appearing small vortices (1, 2, and 4) and stationary vortex (3).

Fig. 6. Velocity field in the section XY at $Z = 1.5$ for variant No. 3: 1) lower vortex

For Re = 500, the flow becomes complicated, nonstationary, and periodic (Fig. 3). Figure 4 shows the calculation results for Re = 500 for variant No. 1 in the section XZ ($Y = 1.5$). As for Re = 100, the gas enters the computational domain as a jet, moves toward the sphere, collides with it, and takes the shape of a dome. At definite time intervals in the section XZ ($Y = 1.5$), small vortices (vortex 1) are formed on both sides of the incoming gas jet; these vortices are then transferred from by the gas flow from the front wall of the volume to the rear one and join with the stationary vortex 3 located there. On each side of the jet, up to three vortices (vortices 1–3) can exist simultaneously. This vortex system replaces the large vortices which occupied the entire space between the front and the rear faces of the volume for Re = 100. As in the case of Re = 100, between the sphere and the rear face of the domain considered, there is a separation zone, but in this case it has a more complex structure: on the edges of its rear part there are two small vortices (vortex 4).

Figure 5 shows the velocity field in the section XY ($Z = 1.5$) for variant No. 2 at Re = 500. Reaching the sphere, the incident flow divides into the upper and lower parts. The upper half of the flow continues moving toward the outlets, and the lower part of the gas jet rapidly changes its direction and moves to the lower wall. Small vortices 1 and 2 are formed periodically on both sides of the gas jet entering the volume. Next, the upper vortex moves along the gas jet to the outlets, and the lower one to the lower wall where it joins the stationary vortex 3 located there. In the rear part of the sphere, at the site of separation of the incident flow, there is also periodic formation of vortices (vortex 4), which are separated from the sphere and carried away by the gas flow toward the outlets.

Figure 6 shows the velocity fields in the section XY ($Z = 1.5$) for variant No. 3 (the sphere touches the lower plane) at Re = 500. In this case, the flow is similar to the flow of variant No. 2 but vortex 1 is destroyed on reaching the sphere.

8. Conclusions. A variant of the finite-volume method was considered and used to model viscous gas flow in a volume having perforated walls and containing a sphere.

The calculation results agree with both experimental and theoretical data.

Viscous gas flow in a volume having perforated walls and containing one sphere was investigated for Re = 100 and 500 and M = 0.6. For each variant of the sphere position, the velocity fields were given and the flow pattern and vortex formation were analyzed.

REFERENCES

1. K. S. Basniev, N. M. Dmitriev, and G. D. Rozenberg, *Oil and Gas Hydromechanics* [in Russian], Institute of Computer Investigations, Moscow–Izhevsk (2005).
2. A. M. Lipanov, "Method of numerical solution of the equations of hydromechanics in a multiply connected domains (First communication)," *Mat. Model.*, **18**, No. 12, 3–18 (2006).
3. L. G. Loitsyanskii, *Mechanics of Liquids and Gases*, Pergamon Press, Oxford–New York (1966).
4. D. V. Beklemishev, *Course in Analytical Geometry and Linear Algebra* [in Russian], Fizmatlit, Moscow (2000).
5. M. A. Lavrent'ev and B. V. Shabat, *Methods of the Theory of Functions of a Complex Variable* [in Russian], Lan', St. Petersburg (2002).
6. E. Kamke, *Handbook of Ordinary Differential Equations*, Chelsea Publ. (1974).
7. L. I. Sedov, *Mechanics of Continuous Media* [in Russian], Vols. 1 and 2, Lan', St. Petersburg (2002).
8. A. A. Samarskii and P. N. Vabishchevich, *Numerical Methods for Solving Problems of Diffusion Convection* [in Russian], Editorial URSS, Moscow (2004).
9. A. M. Lipanov, Y. F. Kisarov, and I. G. Klyuchnikov, *Numerical Experiment in Classical Hydromechanics of Turbulent Flows* [in Russian], Ural Division, Russian Academy of Sciences, Ekaterinburg (2001).
10. A. T. Fedorchenko, "Numerical investigation of nonstationary subsonic flows of viscous gas in a suddenly broadening plane channel," *Izv. Akad. Nauk SSSR, Mekh. Zhidk. Gaza*, No. 4, 32–41 (1988).
11. V. M. Verzhbitskii, *Foundations of Numerical Methods* [in Russian], Vysshaya Shkola, Moscow (2002).
12. A. M. Lipanov, Y. F. Kisarov, and I. G. Klyuchnikov, "Class of high-accuracy difference schemes for direct modeling of turbulent flows with Reynolds numbers $\mathrm{Re} = 10^5$," in: *Use of Mathematical Modeling to Solve Problems in Science and Engineering*, Proc. Sci. Conf., Inst. of Appl. Mech., Izhevsk (1996), pp. 81–102.
13. H. Schlichting, *Boundary Layer Theory*, McGraw Hill, New York (1959).
14. M. M. Gorokhov, "Mathematical modeling of flow and combustion of solid propellant granules in turbulent flows," Doct. Dissertation in Phys.-Math. Sci., Izhevsk (2005).